# Total Deep Variation for Linear Inverse Problems (Supplementary Material)

Erich Kobler† Alexander Effland† Karl Kunisch° Thomas Pock†

†Graz University of Technology °University of Graz

## A. Notation and mathematical preliminaries

In this section, we briefly introduce the notation and give a short presentation of the mathematical preliminaries required for the proofs. All results can be found in [1, 14].

Let $\Omega \subset \mathbb{R}^l$ be a bounded domain. We denote by $C^0(\overline{\Omega}, \mathbb{R}^n)$ the *set of continuous functions* and by $C^k(\overline{\Omega}, \mathbb{R}^n)$, $k \in \mathbb{N}$, the *set of $k$ times continuously differentiable functions* mapping form $\overline{\Omega}$ to $\mathbb{R}^n$. The corresponding norms are

$$\begin{aligned} \|f\|_{C^0(\overline{\Omega},\mathbb{R}^n)} &\coloneqq \max_{x\in\overline{\Omega}} \|f(x)\|_2, \\ \|f\|_{C^k(\overline{\Omega},\mathbb{R}^n)} &\coloneqq \sum_{|\alpha|\leq k} \|D^\alpha f\|_{C^0(\overline{\Omega},\mathbb{R}^n)}, \end{aligned} \tag{1}$$

respectively. Here, we set $D^\alpha f = (\frac{\partial^{\alpha_1} f}{\partial x_1^{\alpha_1}}, \dots, \frac{\partial^{\alpha_n} f}{\partial x_n^{\alpha_n}})^\top$ for a multi-index $\alpha = (\alpha_1, \dots, \alpha_n) \in \mathbb{N}_0^n$ with $|\alpha| = \sum_{i=1}^n \alpha_i$. We define the *Hölder space* as

$$C^{k,s}(\overline{\Omega}, \mathbb{R}^n) \coloneqq \{f \in C^k(\overline{\Omega}, \mathbb{R}^n) : \|f\|_{C^{k,s}(\overline{\Omega},\mathbb{R}^n)} < \infty\} \tag{2}$$

for $k \in \mathbb{N}$ and $s \in (0, 1]$, where the Hölder norm is

$$\|f\|_{C^{k,s}(\overline{\Omega},\mathbb{R}^n)} \coloneqq \|f\|_{C^k(\overline{\Omega},\mathbb{R}^n)} + \sup_{\substack{x,y\in\overline{\Omega}\\ x\neq y}} \frac{\|f(x) - f(y)\|_2}{\|x - y\|_2^s}. \tag{3}$$

For $1 \leq p < \infty$, the *Lebesgue space* $L^p(\Omega, \mathbb{R}^n)$ is the set of all measurable mappings from $\Omega$ to $\mathbb{R}^n$ such that $\|f\|_{L^p(\Omega,\mathbb{R}^n)} < \infty$, where

$$\|f\|_{L^p(\Omega,\mathbb{R}^n)} \coloneqq \left(\int_\Omega \|f(x)\|_2^p \,\mathrm{d}x\right)^{\frac{1}{p}}. \tag{4}$$

The *Sobolev space* $H^m(\Omega, \mathbb{R}^n)$ with $m \in \mathbb{N}$ is the set of all functions $f \in L^2(\Omega, \mathbb{R}^n)$ such that for all $\alpha \in \mathbb{N}_0^n$ with $|\alpha| \leq m$ a function $f^{(\alpha)} \in L^2(\Omega, \mathbb{R}^n)$ exists satisfying

$$\int_\Omega \langle D^\alpha \eta, f\rangle \,\mathrm{d}x = (-1)^{|\alpha|} \int_\Omega \langle \eta, f^{(\alpha)}\rangle \,\mathrm{d}x \tag{5}$$

for all smooth functions $\eta : \Omega \to \mathbb{R}^n$ with compact support. The space $H^m(\Omega, \mathbb{R}^n)$ is endowed with the norm

$$\|f\|_{H^m(\Omega,\mathbb{R}^n)} \coloneqq \sum_{|\alpha|\leq m} \|f^{(\alpha)}\|_{L^2(\Omega,\mathbb{R}^n)}. \tag{6}$$

In what follows, we list several theorems for later reference:

**Theorem A.1.** *We assume that for $x_{\text{init}} \in \mathbb{R}^n$, $g \in C^0(\mathbb{R} \times \mathbb{R}^n, \mathbb{R}^n)$ and each $T > 0$ there are constants $C_1(T), C_2(T) \in (0, \infty)$ such that*

$$\|g(t, x)\|_2 \leq C_1(T) + C_2(T)\|x\|_2 \tag{7}$$

*for all $(t, x) \in [0, T] \times \mathbb{R}^n$. Then all solutions of the initial value problem $\dot{x}(t) = g(t, x)$ with $x(0) = x_{\text{init}}$ are defined for all $t \geq 0$.*

*Proof.* See [14, Theorem 2.17]. □

**Theorem A.2** (Grönwall's inequality)**.** *Suppose that the functions $y, \alpha, \beta \in C^0([0, T], \mathbb{R})$ satisfy*

$$y(t) \leq \alpha(t) + \int_0^t \beta(s)y(s) \,\mathrm{d}s \tag{8}$$

*for all $t \in [0, T]$. If $\alpha$ is monotonically increasing (i.e. $\alpha(s) \leq \alpha(t)$ for $s \leq t \in [0, T]$) and $\beta \geq 0$, then*

$$y(t) \leq \alpha(t) \exp\left(\int_0^t \beta(s) \,\mathrm{d}s\right) \tag{9}$$

*for all $t \in [0, T]$.*

*Proof.* See [14, Lemma 2.7]. □

Next, we present special cases of important results in functional analysis tailored to our particular application.

**Definition A.1.** A sequence $\{g_k\}_{k\in\mathbb{N}}$ in $H^m(\Omega, \mathbb{R}^n)$ converges weakly to $g \in H^m(\Omega, \mathbb{R}^n)$ (denoted by $g_k \rightharpoonup g$) if for every element $g^*$ of the dual space of $H^m(\Omega, \mathbb{R}^n)$ $g^*(g_k) \to g^*(g)$ as $k \to \infty$.

**Theorem A.3.** *Let $I \subset \mathbb{R}$ be a bounded and open interval and $\{g_k\}_{k\in\mathbb{N}}$ in $H^m(I,\mathbb{R}^n)$ be a uniformly bounded sequence in $H^m(I,\mathbb{R}^n)$, i.e. there exists a constant $C > 0$ such that $\|g_k\|_{H^m(I,\mathbb{R}^n)} < C$ for all $k \in \mathbb{N}$. Then there exists a subsequence $\{g_{k_l}\}_{l\in\mathbb{N}}$ of $\{g_k\}_{k\in\mathbb{N}}$ and $g \in H^m(I,\mathbb{R}^n)$ such that $g_{k_l} \rightharpoonup g$ in $H^m(I,\mathbb{R}^n)$ as $l \to \infty$.*

*Proof.* See [2, Chapter 8]. □

**Theorem A.4** (Sobolev embedding theorem)**.** *Let $I \subset \mathbb{R}$ be a bounded and open interval. If $k, m \in \mathbb{N}$ and $\alpha \in (0,1)$ satisfy $m - \frac{1}{2} > k + \alpha$, then the operator $\mathrm{Id} : H^m(I,\mathbb{R}^n) \to C^{k,\alpha}(\overline{I},\mathbb{R}^n)$ is continuous and compact. In particular, for every $g \in H^m(I,\mathbb{R}^n)$ there exists a function $\hat{g} \in C^{k,\alpha}(\overline{I},\mathbb{R}^n)$ that coincides with $g$ almost everywhere such that*

$$\|\hat{g}\|_{C^{k,\alpha}(\overline{I},\mathbb{R}^n)} \leq C\|g\|_{H^m(I,\mathbb{R}^n)}. \tag{10}$$

*The constant $C$ solely depends on $k$, $m$, $I$ and $\alpha$.*

*Proof.* See [2, Theorem 10.13]. □

## B. Existence of solutions

In this section, we briefly recall the functional analytic setting of the optimal control problem. Afterwards, we present the proof for the existence of minimizers of the optimal control problem.

Throughout this section, we consider the data fidelity term $\mathcal{D}(x,z) = \frac{1}{2}\|Ax - z\|_2^2$ for a fixed task-dependent $A \in \mathbb{R}^{lC\times nC}$ and fixed $z \in \mathbb{R}^{lC}$. The total deep variation $\mathcal{R}$ is parametrized by $\theta \in \Theta$, where $\Theta \subset \mathbb{R}^p$ is a compact and convex set of admissible training parameters. We highlight that the building blocks of $\mathcal{R}$ are convolutional layers at different scales and the smooth log-student-t-distribution of the form $\phi(x) = \frac{1}{2\nu}\log(1+\nu x^2)$ for $\nu > 0$. In particular, this structure implies

$$\|\nabla_1 \mathcal{R}(x,\theta)\|_2 \leq C_{\mathcal{R}}(\theta,\nu)\|x\|_2 \tag{11}$$

for a constant $C_{\mathcal{R}}(\theta,\nu) > 0$ depending on $\theta$ and $\nu$. We define the energy functional as

$$\mathcal{E}(x,\theta,z) \coloneqq \mathcal{D}(x,z) + \mathcal{R}(x,\theta). \tag{12}$$

Then, the gradient flow for the finite time interval $(0,T)$ is

$$\begin{aligned}\dot{\tilde{x}}(t) &= -\nabla_1 \mathcal{E}(\tilde{x}(t),\theta,z) = f(\tilde{x}(t),\theta,z) &(13)\\ &\coloneqq -A^\top(A\tilde{x}(t) - z) - \nabla_1 \mathcal{R}(\tilde{x}(t),\theta) &(14)\end{aligned}$$

for $t \in (0,T)$, where $\tilde{x}(0) = x_{\mathrm{init}}$ for a fixed initial value $x_{\mathrm{init}} \in \mathbb{R}^{nC}$. Here, $\tilde{x} : [0,T] \to \mathbb{R}^{nC}$ denotes the differentiable flow of $\mathcal{E}$, and $T > 0$ refers to the time horizon. We assume that $T \in [0, T_{\max}]$ for a fixed $T_{\max} > 0$. To formulate optimal stopping, we exploit the reparametrization $x(t) = \tilde{x}(tT)$, which results for $t \in (0,1)$ in the equivalent gradient flow formulation

$$\dot{x}(t) = Tf(x(t),\theta,z), \qquad x(0) = x_{\mathrm{init}}. \tag{15}$$

For fixed $N \in \mathbb{N}$, let $(x^i_{\mathrm{init}}, y^i, z^i)_{i=1}^N \in (\mathbb{R}^{nC} \times \mathbb{R}^{nC} \times \mathbb{R}^{lC})^N$ be a collection of $N$ triplets of initial-target image pairs, and observed data independently drawn from a task-dependent fixed probability distribution. Let $l : \mathbb{R}^{nC} \to \mathbb{R}_0^+$ be a convex, twice continuously differentiable and coercive (i.e. $\lim_{\|x\|_2\to\infty} l(x) = +\infty$) function. Then, the sampled optimal control problem reads as

$$\inf_{T\in[0,T_{\max}],\,\theta\in\Theta} \left\{ J(T,\theta) \coloneqq \frac{1}{N}\sum_{i=1}^N l(x^i(1) - y^i) \right\} \tag{16}$$

subject to the state equation for each sample

$$\dot{x}^i(t) = Tf(x^i(t),\theta,z^i), \qquad x^i(0) = x^i_{\mathrm{init}} \tag{17}$$

for $i = 1,\dots,N$ and $t \in (0,1)$. The next theorem ensures the existence of solutions to this optimal control problem.

**Theorem B.1** (Existence of solutions)**.** *The minimum in (16) subject to the side conditions (17) is attained.*

*Proof.* Without restriction, we consider the case $N = 1$ and omit the superscript. Taking into account (11) we can estimate as follows:

$$\begin{aligned}&\|Tf(x,\theta,z)\|_2\\ \leq& T(\|A\|_2\|z\|_2) + T(\|A\|_2^2 + C_{\mathcal{R}}(\theta,\nu))\|x\|_2. &(18)\end{aligned}$$

Thus, Theorem A.1 implies that $[0,1]$ is contained in the maximum domain of existence of the state equation (17) for any initial value $x_{\mathrm{init}} \in \mathbb{R}^n$. Let $(T_j,\theta_j) \in [0,T_{\max}] \times \Theta$ be a minimizing sequence for $J$ with an associated state $x_j \in C^1([0,1],\mathbb{R}^n)$ such that (17) with $(T,\theta)$ replaced by $(T_j,\theta_j)$ holds true. Due to the compactness of $[0,T_{\max}]$ and $\Theta$ we can deduce the existence of a subsequence (not relabeled) such that $(T_j,\theta_j) \to (T,\theta) \in [0,T_{\max}] \times \Theta$. Then, Theorem A.2 in conjunction with (18) implies the uniform boundedness of $\|x_j(t)\|_2$ and thus also $\|\dot{x}_j(t)\|_2$ for all $t \in [0,1]$ and all $j \in \mathbb{N}$. In particular, the sequence $\{x_j\}_{j\in\mathbb{N}}$ is uniformly bounded in the Hilbert space $H^1((0,1),\mathbb{R}^n)$. Thus, taking into account Theorem A.3 we can infer that a subsequence (not relabeled) converges weakly in $H^1((0,1),\mathbb{R}^n)$ to $x \in H^1((0,1),\mathbb{R}^n)$. Theorem A.4 ensures the compact embedding of $H^1((0,1),\mathbb{R}^n)$ into $C^0([0,1],\mathbb{R}^n)$, which implies $x_j \to x$ in $C^0([0,1],\mathbb{R}^n)$ and $x(0) = x_{\mathrm{init}}$. Since $f$ is a smooth function, we can even conclude $x \in C^1([0,1],\mathbb{R}^n)$ due to the general theory of ordinary differential equations presented in [7, Chapter I]. Note that $x$ is actually the unique solution to (17). This follows from the convergence of $x_j \to x$ in $C^0([0,1],\mathbb{R}^n)$ and

the smoothness of $f$. Finally, the theorem follows from the continuity of $l$, i.e.

$$\begin{aligned}&\lim_{j\to\infty} J(T_j,\theta_j) = \lim_{j\to\infty} l(x_j(1)-y)\\ =&l(x(1)-y) = J(T,\theta),\end{aligned} \tag{19}$$

where we used the uniform convergence of $x_j \to x$ in $C^0([0,1],\mathbb{R}^n)$. □

## C. Discretized optimal control problem

In this section, we present details for the fully discrete formulation of the sampled optimal control problem. The state equation (17) is discretized using a semi-implicit scheme resulting in

$$x^i_{s+1} = x^i_s - \tfrac{T}{S}A^\top(Ax^i_{s+1} - z^i) - \tfrac{T}{S}\nabla_1\mathcal{R}(x^i_s,\theta) \in \mathbb{R}^{nC} \tag{20}$$

for $s = 0,\dots,S-1$ and $i = 1,\dots,N$, where the *depth* $S \in \mathbb{N}$ is a priori fixed. This equation is equivalent to $x^i_{s+1} = \widetilde{f}(x^i_s,T,\theta,z^i)$ with

$$\begin{aligned}\widetilde{f}(x,T,\theta,z) &\coloneqq B(T)^{-1}(x + \tfrac{T}{S}(A^\top z - \nabla_1\mathcal{R}(x,\theta))),\\ B(T) &\coloneqq \mathrm{Id} + \frac{T}{S}A^\top A.\end{aligned} \tag{21}$$

The initial state satisfies $x^i_0 = x^i_{\text{init}} \in \mathbb{R}^{nC}$. Then, the discretized sampled optimal control problem reads as

$$\inf_{T\in[0,T_{\max}],\,\theta\in\Theta}\left\{J_S(T,\theta) \coloneqq \frac{1}{N}\sum_{i=1}^N l(x^i_S - y^i)\right\} \tag{22}$$

subject to $x^i_{s+1} = \widetilde{f}(x^i_s,T,\theta,z^i)$. We define the Lagrange functional $L_S : (\mathbb{R}^{nC})^{N(S+1)} \times [0,T_{\max}] \times \Theta \times (\mathbb{R}^{lC})^N \times (\mathbb{R}^{nC})^{N(S+1)} \to \mathbb{R}$ as follows:

$$\begin{aligned}(x,T,\theta,z,p) \mapsto J_S(T,\theta) &+ \sum_{i=1}^N \langle p^i_0, x^i_0 - x^i_{\text{init}}\rangle\\ &+ \sum_{s=0}^{S-1}\sum_{i=1}^N \langle p^i_{s+1}, x^i_{s+1} - \widetilde{f}(x^i_s,T,\theta,z^i)\rangle.\end{aligned} \tag{23}$$

The discretization of the associated adjoint equation is now implied by the discrete Pontryagin maximum principle:

**Theorem C.1.** *Let $(\overline{T},\overline{\theta})$ be a pair of optimal control parameters for (22) with the corresponding state equation $\{\overline{x}^i_s\}^{i=1,\dots,N}_{s=0,\dots,S}$. We define the Hamiltonian*

$$\begin{aligned}H : \mathbb{R}^{nC}\times\mathbb{R}^{nC}\times[0,T_{\max}]\times\Theta\times\mathbb{R}^{lC} &\to \mathbb{R},\\ (x,p,T,\theta,z) &\mapsto \langle p, \widetilde{f}(x,T,\theta,z)\rangle.\end{aligned} \tag{24}$$

*If it is further assumed that $\nabla\widetilde{f}(\overline{x}^i_s,\overline{T},\overline{\theta},z^i)$ has full rank for all $i = 1,\dots,N$ and $s = 0,\dots,S$, then there exists an adjoint process $\{\overline{p}^i_s\}^{i=1,\dots,N}_{s=0,\dots,S}$ such that*

$$\begin{aligned}\overline{x}^i_{s+1} &= \nabla_2 H(\overline{x}^i_s,\overline{p}^i_{s+1},\overline{T},\overline{\theta},z^i),\\ \overline{x}^i_0 &= x^i_{\text{init}},\\ \overline{p}^i_s &= \nabla_1 H(\overline{x}^i_s,\overline{p}^i_{s+1},\overline{T},\overline{\theta},z^i),\\ \overline{p}^i_S &= -\frac{1}{N}\nabla l(\overline{x}^i_S - y^i).\end{aligned} \tag{25}$$

*Finally, the solution is optimal in the sense that*

$$\sum_{i=1}^N H(\overline{x}^i_s,\overline{p}^i_{s+1},\overline{T},\overline{\theta},z^i) \geq \sum_{i=1}^N H(\overline{x}^i_s,\overline{p}^i_{s+1},T,\theta,z^i) \tag{26}$$

*for all $T \in [0,T_{\max}]$ and $\theta \in \Theta$.*

*Proof.* For a complete proof, see [11, Theorem 3] and [8]. In what follows, we give a heuristic justification for the definition of the Hamiltonian. To this end, we consider the Lagrange functional $L_S$ with multipliers $\{p^i_s\}^{i=1,\dots,N}_{s=0,\dots,S}$:

$$\begin{aligned}&L_S(x,T,\theta,z,p)\\ =&\frac{1}{N}\sum_{i=1}^N l(x^i_S - y^i) + \sum_{i=1}^N\langle p^i_0, x^i_0 - x^i_{\text{init}}\rangle\\ &+\sum_{s=0}^{S-1}\sum_{i=1}^N\left(\langle p^i_{s+1},x^i_{s+1}\rangle - H(x^i_s,p^i_{s+1},T,\theta,z^i)\right).\end{aligned} \tag{27}$$

Taking the derivatives with respect to $\{x^i_s\}^{i=1,\dots,N}_{s=0,\dots,S}$ and $\{p^i_s\}^{i=1,\dots,N}_{s=0,\dots,S}$ yields (25). □

Thus, (25) readily implies

$$\begin{aligned}\overline{p}^i_s &= \nabla_1 H(\overline{x}^i_s,\overline{p}^i_{s+1},\overline{T},\overline{\theta},z^i)\\ &= (\mathrm{Id} - \tfrac{\overline{T}}{S}\nabla_1^2\mathcal{R}(\overline{x}^i_s,\overline{\theta}))(\mathrm{Id} + \tfrac{\overline{T}}{S}A^\top A)^{-1}\overline{p}^i_{s+1},\\ \overline{p}^i_S &= -\frac{1}{N}\nabla l(\overline{x}^i_S - y^i).\end{aligned} \tag{28}$$

The next theorem states an exact computable condition for the optimal stopping time, which is of vital importance for the numerical optimization:

**Theorem C.2** (Optimality condition)**.** *Let $(\overline{T},\overline{\theta})$ be a stationary point of $J_S$ with associated states $\overline{x}^i_s$ and adjoint states $\overline{p}^i_s$ satisfying (20) and (28). We further assume that $\nabla\widetilde{f}(\overline{x}^i_s,\overline{T},\overline{\theta},z^i)$ has full rank for all $i = 1,\dots,N$ and $s = 0,\dots,S$. Then, we have*

$$-\frac{1}{N}\sum_{s=0}^{S-1}\sum_{i=1}^N\langle\overline{p}^i_{s+1}, B(\overline{T})^{-1}(\overline{x}^i_{s+1} - \overline{x}^i_s)\rangle = 0. \tag{29}$$

*Proof.* We compute the derivative of $\widetilde{f}(x_s^i, T, \theta, z^i)$ with respect to $T$:

$$\begin{aligned}
&\nabla_2 \widetilde{f}(x_s^i, T, \theta, z^i) \\
=&\tfrac{1}{S} B(T)^{-1} \Big( A^\top z - \nabla_1 \mathcal{R}(x_s^i, \theta) \\
&- A^\top A B(T)^{-1} (x_s^i + \tfrac{T}{S}(A^\top z - \nabla_1 \mathcal{R}(x_s^i, \theta))) \Big) \\
=&\frac{1}{T} B(T)^{-1} (x_{s+1}^i - x_s^i),
\end{aligned} \tag{30}$$

where we use

$$\tfrac{\mathrm{d}}{\mathrm{d}T}(B(T)^{-1}) = -B(T)^{-1} \left( \tfrac{\mathrm{d}}{\mathrm{d}T} B(T) \right) B(T)^{-1}. \tag{31}$$

The existence of the Lagrange multiplier $p$ is readily implied by the rank condition of $\nabla \widetilde{f}$ [10, Chapter 1]. At the optimum $(\overline{x}, \overline{T}, \overline{\theta}, z, \overline{p})$ the Lagrange functional $L_S$ satisfies the following optimality condition with respect to $T$:

$$\begin{aligned}
&\nabla_2 L_S(\overline{x}, \overline{T}, \overline{\theta}, z, \overline{p}) \\
=& - \sum_{s=0}^{S-1} \sum_{i=1}^{N} \langle \overline{p}_{s+1}^i, \nabla_2 \widetilde{f}(\overline{x}_s^i, \overline{T}, \overline{\theta}, z^i) \rangle \\
=& - \sum_{s=0}^{S-1} \sum_{i=1}^{N} \langle \overline{p}_{s+1}^i, \tfrac{1}{\overline{T}} B(\overline{T})^{-1} (\overline{x}_{s+1}^i - \overline{x}_s^i) \rangle,
\end{aligned} \tag{32}$$

which readily implies (29). □

In the case of image denoising, the scaling $B(\overline{T})$ in the optimality condition (29) is neglected.

An important property of any learning based method is the dependency of the learned parameters with respect to different training datasets [5].

**Theorem C.3.** *Let $(T, \theta), (\widetilde{T}, \widetilde{\theta})$ be two pairs of control parameters obtained from two different training datasets. We denote by $x, \widetilde{x} \in (\mathbb{R}^{nC})^{(S+1)}$ two solutions of the state equation with the same observed data $z$ and initial condition $x_{\text{init}}$, i.e.*

$$x_{s+1} = \widetilde{f}(x_s, T, \theta, z), \quad \widetilde{x}_{s+1} = \widetilde{f}(\widetilde{x}_s, \widetilde{T}, \widetilde{\theta}, z) \tag{33}$$

*for $s = 1, \dots, S-1$ and $x_0 = \widetilde{x}_0 = x_{\text{init}}$. Let $L_{\mathcal{R}}$ be the Lipschitz constant of $\mathcal{R}$, i.e.*

$$\|\nabla_1 \mathcal{R}(x, \theta) - \nabla_1 \mathcal{R}(\widetilde{x}, \widetilde{\theta})\|_2 \leq L_{\mathcal{R}} \left\| \begin{pmatrix} x \\ \theta \end{pmatrix} - \begin{pmatrix} \widetilde{x} \\ \widetilde{\theta} \end{pmatrix} \right\|_2 \tag{34}$$

*for all $x, \widetilde{x} \in \mathbb{R}^{nC}$ and all $\theta, \widetilde{\theta} \in \Theta$. Then,*

$$\begin{aligned}
&\|x_{s+1} - \widetilde{x}_{s+1}\|_2 \\
\leq& \|B(T)^{-1} - B(\widetilde{T})^{-1}\|_2 \Big( \|x_s\|_2 + \tfrac{T}{S} \|A^\top z\|_2 \\
&+ \tfrac{T}{S} \|\nabla_1 \mathcal{R}(x_s, \theta)\|_2 \Big) + \|B(\widetilde{T})^{-1}\|_2 \Big( \|x_s - \widetilde{x}_s\|_2 \\
&+ \tfrac{|T - \widetilde{T}|}{S} \|A^\top z\|_2 + \tfrac{|T - \widetilde{T}|}{S} \|\nabla_1 \mathcal{R}(\widetilde{x}_s, \widetilde{\theta})\|_2 \\
&+ \tfrac{T}{S} L_{\mathcal{R}} \|(x_s, \theta)^\top - (\widetilde{x}_s, \widetilde{\theta})^\top\|_2 \Big).
\end{aligned} \tag{35}$$

*Proof.* Let $g(x, T, \theta) \coloneqq x + \frac{T}{S} A^\top z - \frac{T}{S} \nabla_1 \mathcal{R}(x, \theta)$. By definition,

$$\begin{aligned}
x_{s+1} &= B(T)^{-1} g(x_s, T, \theta), \\
\widetilde{x}_{s+1} &= B(\widetilde{T})^{-1} g(\widetilde{x}_s, \widetilde{T}, \widetilde{\theta}).
\end{aligned} \tag{36}$$

Thus, we can estimate the upper bound as follows:

$$\begin{aligned}
&\|x_{s+1} - \widetilde{x}_{s+1}\|_2 \\
=& \|B(T)^{-1} g(x_s, T, \theta) - B(\widetilde{T})^{-1} g(\widetilde{x}_s, \widetilde{T}, \widetilde{\theta})\|_2 \\
\leq& \|B(T)^{-1} - B(\widetilde{T})^{-1}\|_2 \Big( \|x_s\|_2 + \tfrac{T}{S} \|A^\top z\|_2 \\
&+ \tfrac{T}{S} \|\nabla_1 \mathcal{R}(x_s, \theta)\|_2 \Big) + \|B(\widetilde{T})^{-1}\|_2 \Big( \|x_s - \widetilde{x}_s\|_2 \\
&+ \tfrac{|T - \widetilde{T}|}{S} \|A^\top z\|_2 + \tfrac{|T - \widetilde{T}|}{S} \|\nabla_1 \mathcal{R}(\widetilde{x}_s, \widetilde{\theta})\|_2 \\
&+ \tfrac{T}{S} L_{\mathcal{R}} \|(x_s, \theta)^\top - (\widetilde{x}_s, \widetilde{\theta})^\top\|_2 \Big).
\end{aligned} \tag{37}$$

This concludes the proof. □

Hence, this theorem provides a computable upper bound for the norm difference of two states with observed value $z$ and initial value $x_{\text{init}}$ evaluated at the same step $s$, which amounts to a sensitivity analysis w.r.t. the training data.

## D. Additional numerical results

Figure 1 depicts four additional results for the image denoising task computed with $\text{TDV}_{25}^3$ for a noise level $\sigma = 25$. The best results in terms of the PSNR value are obtained for $S = 10$ and are highlighted in red.

Figure 2 shows four image sequences associated with image super-resolution with a scale factor 4. The algorithm generates a transition from the initial upsampled ($S = 0$) to a cartoon-like image with strongly pronounced edges ($S = 20$). Here, the optimal stopping time is image dependent and determines the best image in terms of PSNR value.

## E. Transferring TDV to different linear inverse problems

In this section, we elaborate on how the prior information incorporated in the TDV regularizer can be transferred to different linear inverse problems *without* any adaption of the learnable parameters.

As before, we consider minimizing the variational energy

$$\mathcal{E}(x, \theta, z) \coloneqq \mathcal{D}(x, z) + \mathcal{R}(x, \theta), \tag{38}$$

in which the problem specific data fidelity term

$$\mathcal{D}(x, z) = \frac{\lambda}{2} \|Ax - z\|_2^2 \tag{39}$$

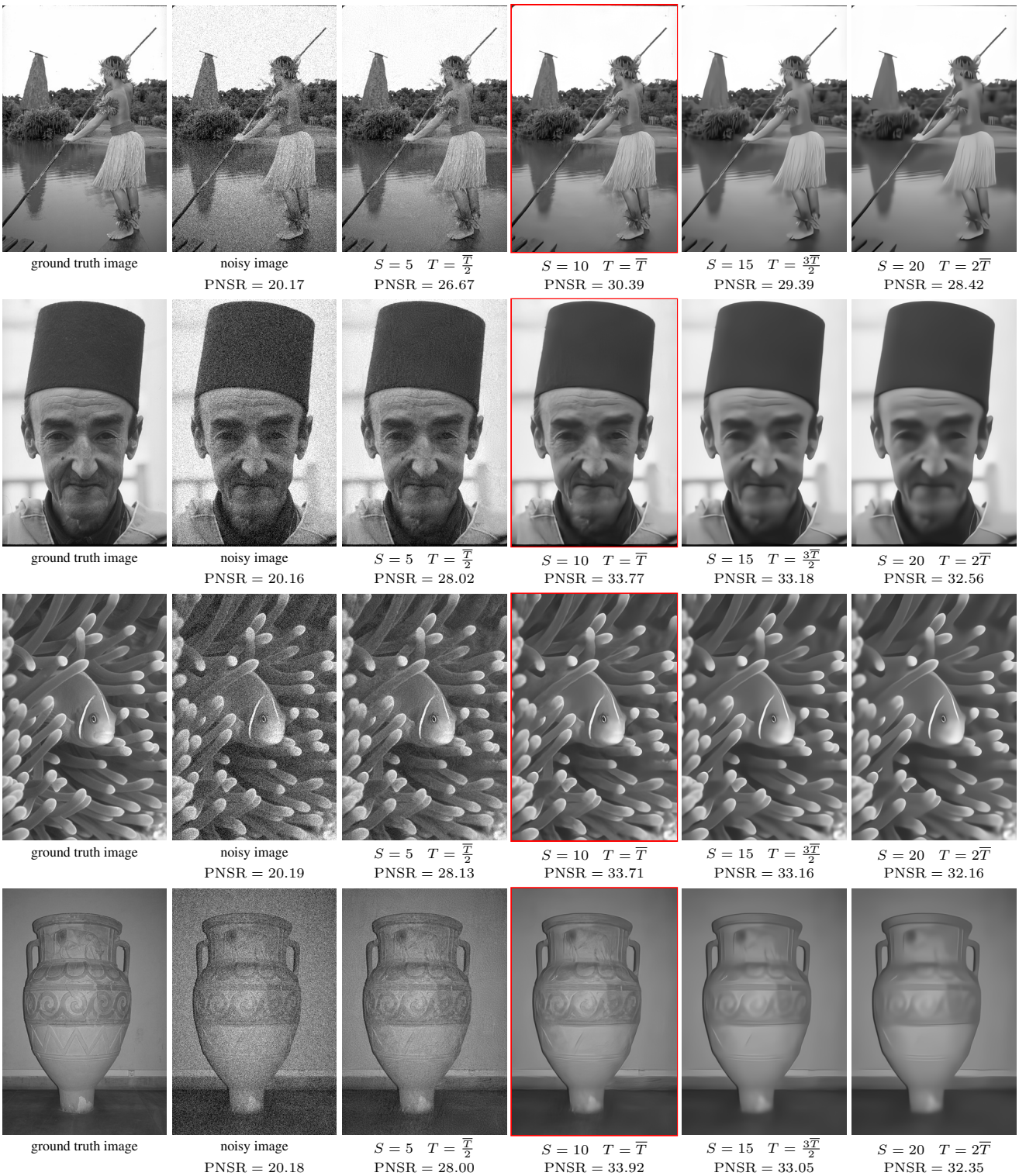


Figure 1. From left to right: Ground truth, noisy input with noise level $\sigma = 25$ and resulting output of TDV$^3$ for $(S, T) \in \{(5, \frac{\overline{T}}{2}), (10, \overline{T}), (15, \frac{3\overline{T}}{2}), (20, 2\overline{T})\}$, where the optimal stopping time is $\overline{T} = 0.0297$. Note that the best image is framed in red.

is used to estimate an image $x \in \mathbb{R}^{nC}$ from observed measurements $z \in \mathbb{R}^{lC}$. The linear operator $A \in \mathbb{R}^{lC \times nC}$ models the data acquisition process of the inverse problem at hand. The scalar weight $\lambda > 0$ allows to manually bal-

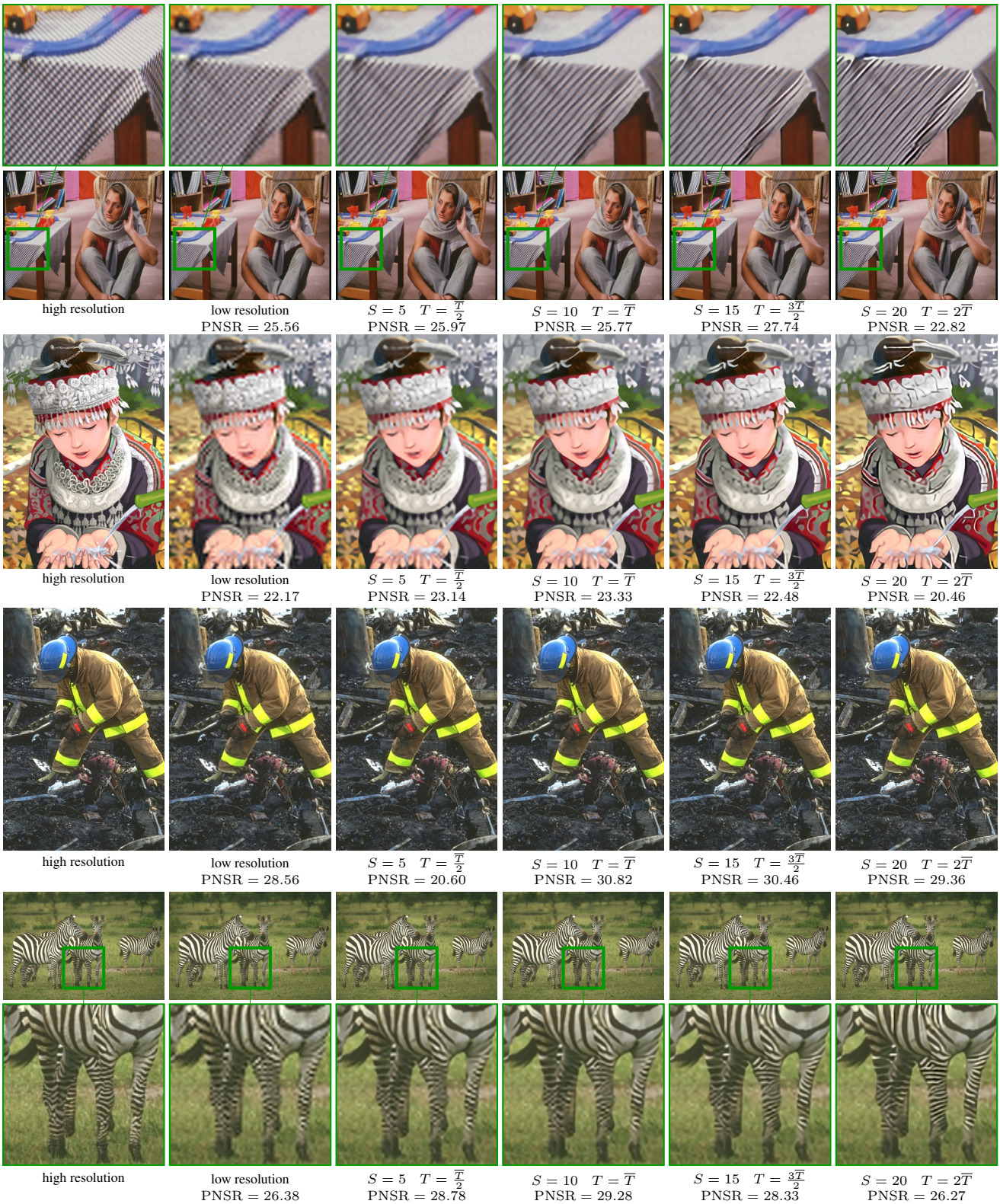


Figure 2. From left to right: High resolution, low resolution with scale factor 4, and resulting output of TDV$^3$ for $(S, T) \in \{(5, \frac{\overline{T}}{2}), (10, \overline{T}), (15, \frac{3\overline{T}}{2}), (20, 2\overline{T})\}$, where the optimal stopping time is $\overline{T} = 0.098$.

**for** $k = 1$ **to** $K$ **do**
  /* over-relaxation */
  $\widehat{x}_k = x_k + \frac{1}{\sqrt{2}}(x_k - x_{k-1})$;
  **while** *True* **do**
    $x_{k+1} = \widehat{x}_k - \frac{1}{L}\nabla_1 \mathcal{E}(\widehat{x}_k, \theta, z)$;
    /* Lipschitz backtracking */
    $q = \langle x_{k+1} - \widehat{x}_k, \nabla \mathcal{E}(\widehat{x}_k, \theta, z)\rangle + \frac{L}{2}\|x_{k+1} - \widehat{x}_k\|_2^2$;
    **if** $\mathcal{E}(x_{k+1}, \theta, z) \leq \mathcal{E}(\widehat{x}_k, \theta, z) + q$ **then**
      $L = \frac{L}{2}$;
      **break**;
    **end**
    **else**
      $L = 2L$;
    **end**
  **end**
**end**

**Algorithm 1:** Accelerated gradient descent with Lipschitz backtracking.

ance the weighting between data fidelity and regularization. To incorporate prior knowledge in the reconstruction process (38), we consider the smooth TDV regularizer $\mathcal{R}(x, \theta)$. Here, we assume that the TDV parameters $\theta$ have already been determined by a previous training process for a different inverse problem (e.g. image denoising) as presented in the paper. As a result, we are able to transfer the regularization strategies obtained by training from data on a different task to another specific restoration/reconstruction problem by just using the learned regularizer.

For given measurements $z \in \mathbb{R}^{lC}$ and previously computed trainable parameters $\theta \in \Theta$ we retrieve the restored image $x$ via

$$\operatorname*{argmin}_{x \in \mathbb{R}^{nC}} \mathcal{E}(x, \theta, z). \tag{40}$$

Since both the data fidelity term and the regularization term are smooth, any convergent first-order gradient method is suitable for optimizing (40). Algorithm 1 lists the applied accelerated gradient descent method with Lipschitz backtracking. We adopt a Lipschitz backtracking strategy to approximate the local Lipschitz constant. Algorithm 1 is known to converge to stationary points of (40) if the number of iterations $K$ is chosen large enough [3, 13].

To sum up, the idea of reusing prior knowledge extracted from data for a different inverse problem by means of a regularizer enables a simple and effective approach that does not require any further training. Next, we demonstrate the applicability of this idea by applying a regularizer learned for gray-scale image denoising to computed tomography (CT) and magnetic resonance imaging (MRI) reconstruction.

## F. Computed tomography

To showcase the effectiveness of the transfer idea introduced in the previous section, we consider the linear inverse problem of angular undersampled two dimensional computed tomography (CT). The task of CT is to reconstruct an image given projection measurements for different acquisition angles. All these measurements are stacked along the angular dimension to form the sinogram $z$. In practice typically $R = 2304$ acquisition angles with 768 projections are considered, thus $z \in \mathbb{R}^{768R}$. In the case of angular undersampled CT [4] only a fraction of the acquisition angles are measured. Here, the goal is to reconstruct the image with a similar quality by incorporating prior knowledge in the form of regularization.

The angular undersampled CT problem can be addressed by considering the data fidelity term

$$\mathcal{D}(x, z) = \frac{\lambda}{2}\|A_R x - z\|_2^2, \tag{41}$$

where $A_R : \mathbb{R}^{R \cdot 768 \times 768 \cdot 768}$ is the linear projection operator acquiring $R$ angles introduced in [6] and $z = A_R y$ is the measured sinogram of the true image $y$. We use the $\text{TDV}^3_{25}$ regularizer trained for image denoising and $S = 10$ without changing its learnable parameters.

We evaluate the qualitative performance of the proposed regularizer transfer approach on a sample slice of the MAYO dataset [12]. The reconstructed images from the fully-sampled, 4/8-fold undersampled sinogram are depicted in Figure 8 in the paper. It is clearly visible that the $\text{TDV}^3_{25}$ regularizer yields reconstructed images of similar quality. Consequently, the regularizer is able to remove the undersampling artifacts while preserving fine details.

## G. Magnetic resonance imaging

In this section, we demonstrate the wide-ranging usability of the proposed approach by transferring the TDV regularizer trained for image denoising to parallel accelerated MRI, which exhibits strong and structured undersampling artifacts.

In detail, in parallel accelerated MRI only a subset of the k-space data of each coil is measured during the acquisition process (for details see [9]). The task in parallel accelerated MRI is the reconstruction of the scanned image $x$ given the undersampled k-space data $z_i$ of each receiver coil $i = 1, \ldots, N_C$. To account for multiple coils, we change the data fidelity term to

$$\mathcal{D}(x, \{z\}_{i=1}^{N_C}) = \frac{\lambda}{2}\sum_{i=1}^{N_C}\|M_R F C_i x - z_i\|_2^2. \tag{42}$$

The linear operator $C_i \in \mathbb{C}^{n \times n}$ weights the complex image estimate by the coil sensitivity map of the $i^{th}$ coil, which

was computed by [15], $F \in \mathbb{C}^{n\times n}$ is the Fourier transform, and $M_R \in \mathbb{C}^{n\times n}$ is an binary mask for $R$-fold undersampling. Here, we consider Cartesian undersampled k-space data as in [9]. As in the previous sections, the scalar weight $\lambda$ needs to be adapted to balance data fidelity and regularization. Despite the large difference between noise artifacts and the undersampling artifacts introduced by Cartesian undersampling, we use the $\text{TDV}^3_{25}$ regularizer trained for image denoising and $S = 10$ to regularize this linear inverse problem.

We perform a qualitative evaluation of the proposed approach on a representative slice of an undersampled MRI knee image. The slice has a resolution of $n = 320 \cdot 320$ pixels, and $N_C = 15$ receiver coils were used during the acquisition. Figure 9 in the paper depicts the results of the accelerated parallel MRI problem using the $\text{TDV}^3_{25}$ regularizer. Although the TDV regularizer was not trained to account for undersampling artifacts, all these artifacts are removed in the reconstructions and only some details in the bone are lost. This highlights the versatility and effectiveness of the proposed TDV regularizer since both challenging medical inverse problems can be properly addressed *without* any fine-tuning of the learned parameters.

## References


[1] Robert A. Adams and John J. F. Fournier. *Sobolev spaces*, volume 140 of *Pure and Applied Mathematics, Amsterdam*. Elsevier/Academic Press, Amsterdam, second edition, 2003. 1

[2] Hans Wilhelm Alt. *Linear functional analysis*. Universitext. Springer-Verlag London, Ltd., London, 2016. 2

[3] Antonin Chambolle and Thomas Pock. An introduction to continuous optimization for imaging. *Acta Numer.*, 25:161–319, 2016. 7

[4] Guang-Hong Chen, Jie Tang, and Shuai Leng. Prior image constrained compressed sensing (PICCS): A method to accurately reconstruct dynamic CT images from highly undersampled projection data sets. *Medical Physics*, 35(2):660–663, 2008. 7

[5] Stuart Geman, Elie Bienenstock, and René Doursat. Neural networks and the bias/variance dilemma. *Neural computation*, 4(1):1–58, 1992. 4

[6] Sungsoo Ha and Klaus Mueller. A look-up table-based ray integration framework for 2-D/3-D forward and back projection in X-ray CT. *IEEE Transactions on Medical Imaging*, 37:361–371, 2018. 7

[7] Jack K. Hale. *Ordinary differential equations*. Robert E. Krieger Publishing Co., Inc., Huntington, N.Y., second edition, 1980. 2

[8] Hubert Halkin. A maximum principle of the Pontryagin type for systems described by nonlinear difference equations. *SIAM J. Control*, 4:90–111, 1966. 3

[9] Kerstin Hammernik, Teresa Klatzer, Erich Kobler, Michael P. Recht, Daniel K. Sodickson, Thomas Pock, and Florian Knoll. Learning a variational network for reconstruction of accelerated MRI data. *Magnetic Resonance in Medicine*, 79(6):3055–3071, 2018. 7, 8

[10] Kazufumi Ito and Karl Kunisch. *Lagrange multiplier approach to variational problems and applications*, volume 15 of *Advances in Design and Control*. Society for Industrial and Applied Mathematics (SIAM), Philadelphia, PA, 2008. 4

[11] Qianxiao Li and Shuji Hao. An optimal control approach to deep learning and applications to discrete-weight neural networks. In *International Conference on Machine Learning*, 2018. 3

[12] Cynthia H. McCollough, Adam C. Bartley, Rickey E. Carter, Baiyu Chen, Tammy A. Drees, Phillip Edwards, David R. Holmes III, Alice E. Huang, Farhana Khan, Shuai Leng, Kyle L. McMillan, Gregory J. Michalak, Kristina M. Nunez, Lifeng Yu, and Joel G. Fletcher. Low-dose CT for the detection and classification of metastatic liver lesions: Results of the 2016 low dose CT grand challenge. *Medical Physics*, 44(10):339–352, 2017. 7

[13] Thomas Pock and Shoham Sabach. Inertial proximal alternating linearized minimization (ipalm) for nonconvex and nonsmooth problems. *SIAM J. Imaging Sci.*, 9(4):1756–1787, 2016. 7

[14] Gerald Teschl. *Ordinary differential equations and dynamical systems*, volume 140 of *Graduate Studies in Mathematics*. American Mathematical Society, Providence, RI, 2012. 1

[15] Martin Uecker, Peng Lai, Mark J. Murphy, Patrick Virtue, Michael Elad, John M. Pauly, Shreyas S. Vasanawala, and Michael Lustig. ESPIRiTan eigenvalue approach to autocalibrating parallel MRI: where SENSE meets GRAPPA. *Magnetic resonance in medicine*, 71(3):990–1001, 2014. 8